Hindawi
Australian Journal of Grape and Wine Research
Volume 2023, Article ID 3923839, 12 pages
https://doi.org/10.1155/2023/3923839

AUSTRALIAN SOCIETY OF VITICULTURE AND OENOLOGY | ASVO

Research Article

A Preliminary Method for Tracking In-Season Grapevine Cluster Closure Using Image Segmentation and Image Thresholding

Manushi Trivedi,[1] **Yuwei Zhou**,[2,3] **Jonathan Hyun Moon**,[4] **James Meyers**,[5] **Yu Jiang**,[1] **Guoyu Lu**,[2] **and Justine Vanden Heuvel**[1]

[1]*Horticulture Section, School of Integrative Plant Science, Cornell University, Ithaca 14853, NY, USA*
[2]*Electrical and Computer Engineering, University of Georgia, Athens 30602, GA, USA*
[3]*Electrical and Computer Engineering, Rochester Institute of Technology, Rochester 14623, NY, USA*
[4]*Department of Computer Science, Cornell University, Ithaca 14853, NY, USA*
[5]*Formerly, Cornell Cooperative Extension, Cornell University, Ithaca 14853, NY, USA*

Correspondence should be addressed to Justine Vanden Heuvel; justine@cornell.edu

Received 10 June 2023; Revised 7 September 2023; Accepted 15 September 2023; Published 30 September 2023

Academic Editor: K. J. Evans

Mapping and monitoring cluster morphology provides insights for disease risk assessment, quality control in wine production, and understanding environmental influences on cluster shape. During the progression of grapevine morphology, cluster closure (CC) (also called bunch closure) is the stage when berries touch one another. This study used mobile phone images to develop a direct quantification method for tracking CC in three grapevine cultivars (Riesling, Pinot gris, and Cabernet Franc). A total of 809 cluster images from fruit set to veraison were analyzed using two image segmentation methods: (i) a Pyramid Scene Parsing Network (PSPNet) to extract cluster boundaries and (ii) Otsu's image thresholding method to calculate % CC based on gaps between the berries. PSPNet produced high accuracy (mean accuracy = 0.98, mean intersection over union (mIoU) = 0.95) with mIoU > 0.90 for both cluster and noncluster classes. Otsu's thresholding method resulted in <2% falsely classified gap and berry pixels affecting quantified % CC. The progression of CC was described using basic statistics (mean and standard deviation) and using a curve fit. The CC curve showed an asymptotic trend, with a higher rate of progression observed in the first three weeks, followed by a gradual approach towards an asymptote. We propose that the *X* value (in this example, number of weeks past berry set) at which the CC progression curve reaches the asymptote be considered as the official phenological stage of CC. The developed method provides a continuous scale of CC throughout the season, potentially serving as a valuable open-source research tool for studying grapevine cluster phenology and factors affecting CC.

1. Introduction

Cluster closure (CC) is typically defined as a phenological stage (modified Eichhorn and Lorenz (E-L) stage 32) [1] when within the cluster berries begin to touch each other. CC is defined as a single phenological stage; however, it actually progresses over a period of many weeks as the cluster changes from a few berries touching one another to a fully closed cluster where all berries are touching other berries. In varieties of Vitis vinifera, higher in-contact berry surface area increases the cluster's susceptibility to diseases such as botrytis bunch rot (Botrytis cinerea) and black rot (Guignardia bidwellii) [2, 3].

Another commonly used term in viticulture is cluster compactness, which is an indicator of the compactness or denseness of the cluster [4]. Cluster compactness is generally quantified as the number of berries per unit length of the rachis [3]. However, it is usually measured post-veraison, whereas CC occurs earlier in the season. Compact clusters are subject to poor air circulation and microcracks in cuticle membranes [5, 6]. There is an assumption in viticulture that compact clusters have an earlier CC; however, we know of

no data that test that hypothesis. The development of a reliable quantification method could help researchers better determine factors that influence the timing of CC.

Conventionally, CC is estimated using a ranking method based on the visual interpretation of visible pedicels (International Organization of Vine and Wine) [7]. This method covers both CC and compactness, as visible pedicels would be reduced in more closed and/or more compact clusters. However, this CC ranking method is subjective with estimates potentially varying among data collectors [7]. Methods of estimating cluster compactness include determining the number of berries per cm rachis or length of laterals [3, 8], amount of water displacement caused by the gaps present between the berries [4], or complex compactness indices based on cluster and pedicel number/weight and/or length [9]. The measurements of the inputs required to quantify cluster closure/compactness have been partially automated; for example, Aquino et al. [12], Coviello et al. [11], and Zabawa et al. [12] developed a direct method for counting the number of berries under field conditions, which is one of the inputs; however, only a small number of studies have effectively estimated rachis length (another crucial input) by generating 3D images from 2D images of clusters acquired in the field [13, 14]. A recent study by Palacios et al. [15] estimated the ratio of the rachis area to cluster area against OIV ranking as an estimator of cluster compactness. However, cluster compactness methods heavily rely on the number of berries, which presumably remain the same after fruit set, and the rachis generally stops elongating after veraison [16], but the berries keep expanding. Thus, tracking CC using cluster compactness indices would be restraining.

Image segmentation techniques have been widely used in viticulture to extract cluster morphological features. Liu et al. [17] used images captured by a mobile phone camera to create a 3D representation of each cluster. Ivorra et al. [18] further classified 3D representations of clusters into berries, background, and gaps using a colour segmentation algorithm in multiple grapevine cultivars. In comparison, Cubero et al. [19] used Bayesian discriminant segmentation to classify the gaps between the berries and estimated cluster compactness using averaged areas of pixels representing gaps at areas above the certain width of the cluster (25%, 50%, and 75% width relative to the cluster central axis). When the 2D image analysis-based cluster compactness methods are compared with 3D scanner-based methods, the authors discovered that 3D image-based methods are constrained by the variations inherent in the dataset, particularly when dealing with loose clusters [20]. This limitation can pose challenges in terms of generalizing these methods to different datasets. 3D images help describe the gaps between the berries in depth from the inner to the outer cluster; however, a simpler solution could be used for CC that suggests the extent to which berry surfaces are touching one another.

The objective of this research was to develop a convenient method for quantifying the progression of CC by tracking the gap area between the berries as percentage area relative to the cluster area using 2D image analysis under field conditions, resulting in a continuous CC scale that can be used as a research tool. Further development and validation of this cluster tracking tool is expected to aid studies of cluster morphology and phenology and may be used for potential applications such as modelling disease infection periods.

2. Methods and Materials

2.1. Study Area and Image Collection. Cluster images were collected in three vineyard blocks. Two blocks (Riesling and Pinot gris) were located in Portland, NY, USA (42°21′10″N, 79°29′27″W), and one block of Cabernet Franc was in Lansing, NY, USA (42°34′23″N, 76°35′44″W). These cultivars are commonly grown in New York State, USA. Clusters from these nonreplicated vineyard blocks were used to develop the CC model and may not have been representative of the same cultivars grown in the broader region. For example, the Cabernet Franc block was particularly of low vigour than at the other sites in the region, yielding looser clusters compared to high-vigor vines. Thus, the inclusion of the low-vigour Cabernet Franc block in the study enabled the testing of the developed tool on both compact and loose clusters. All blocks were managed in the same way using the standard viticultural practices for the region.

Each week starting from fruit set (E-L stage 27), approximately 50 images per cultivar were collected. Within each block, four contiguous panels were selected based on vine uniformity. On each sampling date, basal clusters only were sampled arbitrarily from the four-panel block since grape growers in the region sometimes cluster thin the vines to 1 cluster/shoot. A mobile phone camera with ~9 mega pixels and 96 dots per inch resolution was used. Clusters were imaged from one side/angle while attached to the vine (i.e., clusters were not removed for imaging). A whiteboard was placed behind the cluster to use as a background, with the goal of calculating % CC based on the % white space/gaps present in between the berries. The whiteboard also helped capture clear cluster boundaries and prevented inclusion of nontarget objects such as soil, cover crop, and vine canopy foliage. The images were taken by a hand held mobile phone, without the use of any supplementary lighting, specialized camera equipment, or specific aperture settings during the capture process.

Riesling and Pinot gris images were collected every week for five weeks (June 29, July 6, July 12, July 19, and July 28 in 2021) and Cabernet Franc for seven weeks (July 2, July 11, July 19, July 26, August 3, August 12, and August 23 in 2020). A total of 224, 233, and 325 (total of 809) images were included for Pinot gris, Riesling, and Cabernet Franc, respectively. The first image collection was at the grape phenological stage of the fruit set (E-L stage 27), and the last one was when the clusters were mostly closed (approximately E-L stages 32–34).

2.2. Image Annotation. Following the cluster image collection, 204 images were randomly selected across all samples (total 809 images) depicting different

phenological stages. The images were manually annotated (steps 1 and 2 in Figure 1). Subsequently, an initial segmentation algorithm named the Pyramid Scene Parsing Network (PSPNet) [21] was trained using the original and annotated images to extract the boundaries of the clusters (step 3). The resulting cluster boundaries were then employed to mask the original images, after which additional image processing techniques such as grayscale conversion and contrast enhancements were applied (step 4). Due to the white-coloured background, the berry pixels appeared darker than the surrounding white space/gap pixels in grayscale images. Hence, a second single value-based image segmentation technique, Otsu's image thresholding method [22], was employed to calculate a threshold image value to distinguish between the berry and the gap pixels, utilizing the image histogram distribution (step 5). Subsequently, the images were converted into binary images, where pixels were assigned to either the berry class or the gap class based on the threshold value. Finally, % CC was calculated by determining the ratio of the number of berry pixels to the total cluster area (step 6).

The Computer Vision Annotation Tool (CVAT) (https://cvat.org) was used to annotate 204 images using automatic boundaries' functionality. The automatic boundary detection in CVAT measures the colour and contrast between the user-drawn boundaries and creates the image labels. Images were labelled into two classes: cluster and noncluster. Only cluster boundaries were delineated as a cluster class, and the rest of the image area was labelled as a noncluster class.

2.3. Extraction of Cluster Boundaries. Even though the whiteboard was used as a background, the presence of unwanted objects such as a human hand and similar entities in colour and shape, such as canopy and clusters captured other than the intended one, were there in the image dataset with different zoom-out levels (as shown in Figure 2). In all images (Figure 2), the target cluster is typically positioned at the centre of the overall image and above the whiteboard, despite the presence of objects with similar colours and shapes. Thus, contextual information was very important to extract cluster boundaries accurately. In addition to image context, the size of the cluster compared to the noncluster area is relatively smaller for all images making multiscale information crucial for accurately separating the two classes. Therefore, a semantic image segmentation algorithm capturing contextual and multiscale information was implemented. Semantic image segmentation is a technique where each pixel is assigned to a specific class label; here, it was cluster class and noncluster class. We primarily used PSPNet proposed by Zhao et al. [21] for segmenting the cluster area because of its computational efficiency and multiscale spatial pooling method. However, we also tried DeepLabv3 [23] as another representative benchmark method, and the experimental results can be found on the GitHub page (https://github.com/manushibt/Qunatifying-Grapevine-Cluster-Closure-QCC-.git), along with all codes used in this study.

PSPNet is based on a convolutional neural network (CNN) and can capture multiscale and contextual information of the image dataset. PSPNet utilizes a pyramid pooling module to capture contextual information from different levels of feature maps. The pyramid pooling module divides the feature maps into multiple regions of images into different scales (1×1, 2×2, 3×3, etc.) and then applies pooling operations to capture contextual information within each region. This allows PSPNet to capture multiscale contextual information, from local to global context, which helps improve the segmentation accuracy. The pooled feature maps are then concatenated and further processed to generate the final segmentation map. PSPNet was trained using PaddleSeg [24]. The dataset was divided into training and testing sets using an 80 : 20 ratio. This resulted in 163 out of 209 annotated images being utilized for training, while accuracies were assessed on a testing dataset comprising 41 images. The random distribution of images across these sets aimed to mitigate modelling bias. The model parameters were set as batch size: 4; iteration: 10000; backbone: ResNet50_vd; learning rate: 0.01; and loss: cross entropy. Basic augmentation techniques of image resizing and image flipping were used as a part of PSPNet.

The model was evaluated using two metrics: mean accuracy (mAcc) and mean intersection over union (mIoU) [25]. mAcc gives % of pixels classified correctly for each image in the testing data set, and mIoU shows the ratio of % overall area overlaps between classified and annotated images. Both metrics range from 0 to one. Moreover, precision and recall rates were reported per class. Precision measures the number of correctly classified pixels for each of the classes and recall measures the completeness of the predictions for each of the classes. All metrics ranged from 0 to 1.

2.4. Image Processing and Quantification of % CC. After segmenting images into cluster vs. noncluster class, only the cluster area was extracted by masking the original images with segmented images using the NumPy package in Python [26]. The areas other than the cluster were set to null value. After this step, the masked images could be categorised as berry pixels and the gap pixels. Since the gap pixels were brighter and white in colour, the berry and gap pixels could be separated using an image histogram and a single value-based image thresholding method to classify each pixel into either berry or gap class. Image thresholding is a simple way of image segmentation where a fixed or variable threshold value is used to convert original images into binary images with values 0 or 1. Even though there was a distinct colour difference in the masked image (white and green), a fixed threshold value of red-green-blue (RGB) colour space was not optimal because of the variation in zoom levels of images and the angle of the images causing various shades of green. To standardize the RGB colour space and eliminate variation, the masked images were converted from three-dimensional RGB colour space into one-dimensional grayscale images (step 4 in Figure 1) using the OpenCV package [27]. The grayscale image had only pixel intensity

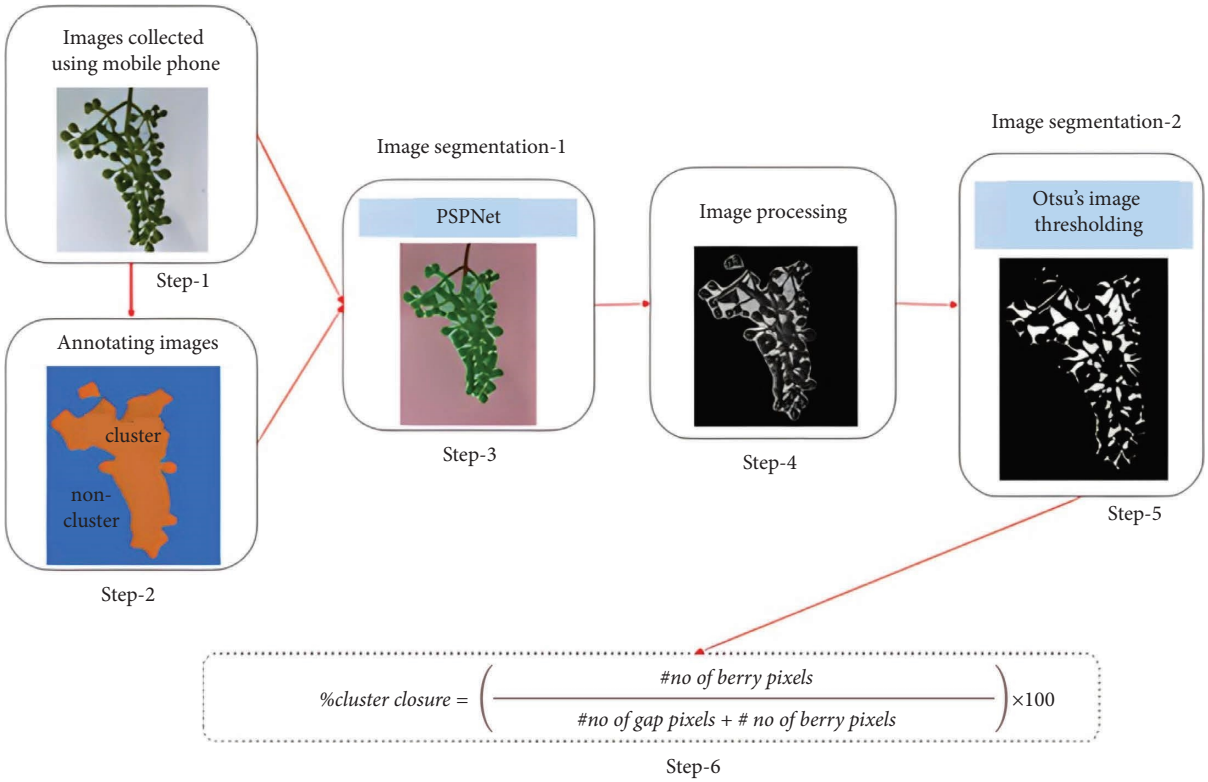

Figure 1: General workflow of the proposed method; steps 1 and 2 include image collection and annotating part of the collected image dataset; step 3 includes running the first image segmentation algorithm (PSPNet) to segment images into the cluster and noncluster class; step 4 includes multiple steps of image processing such as image masking, grayscale conversion, and image contrast enhancement (see methodology section); step 5 is second image segmentation where cluster areas were segmented into berry pixels and gap pixels using Otsu's thresholding method; step 6 uses berry area and gap area to calculate % CC.

values and did not have colour shades (hue and saturation value) information, facilitating further image processing and analysis.

The grayscale images had mostly bimodal image distribution early in the season. The left peak in the distribution exhibits berry pixels with low-intensity values (closer to 0), and the right peak shows gap pixels with high-intensity values (closer to 255) (Figure 3). Otsu's image thresholding method was used to segment these bimodal images into berries and gap class. Otsu's method is an automatic, nonparametric, and unsupervised way to threshold images and classify into two classes, foreground and background [22]. In this method, the probability distribution of image pixels is calculated for each foreground (berries) and background (gaps present between the berries) class. Then, the class variance is calculated for each possible threshold value (0 to 255). The final threshold is the value giving minimum intraclass variance and maximum interclass variance. The thresholding was implemented using the OpenCV package in Python.

The calculated Otsu's threshold value was accurate for early-stage images where a higher number of gap pixels were present indicating clear bimodal image distribution. However, as berries expanded, the number of gap pixels decreased, lowering the magnitude of the right peak into the right tail (Figure 3(c)). This effect was prominent for compact cluster cultivars such as Riesling and Pinot gris. Thus, images captured later in the season had uniform image distribution for these cultivars. Otsu's threshold method performs poorly for unimodal image distribution as it has a larger intraclass variance than the interclass one [28]. In addition, some of the berry pixels were brighter at every phenological stage because of the variations in illumination, image angle, and berry/canopy shading. Combining these reasons, the images closer to CC had falsely classified brighter berry pixels into gap pixels (Figure 4) because Otsu's threshold value was almost in the centre of the image distribution (Figure 3(e)).

The issue of unimodal image distribution was overcome by increasing the contrast using the image-shifting technique. The original image values were shifted left by subtracting the absolute 40 intensity value from the original image intensity values. The number of falsely classified images out of 809 images was calculated for different shifting values, 10, 20, 30, 40, 50, 60, 70, 80, 90, 100, and the value 40 was chosen as it gave the least falsely classified images (1.6% of total images). The number of falsely classified images was calculated using visual interpretation. The highest possible value for shifting was set to 100 as the difference between Otsu's threshold and desired threshold values was approximately 100. By increasing the contrast, the brighter pixels of the berries were darkened. The increased contrast

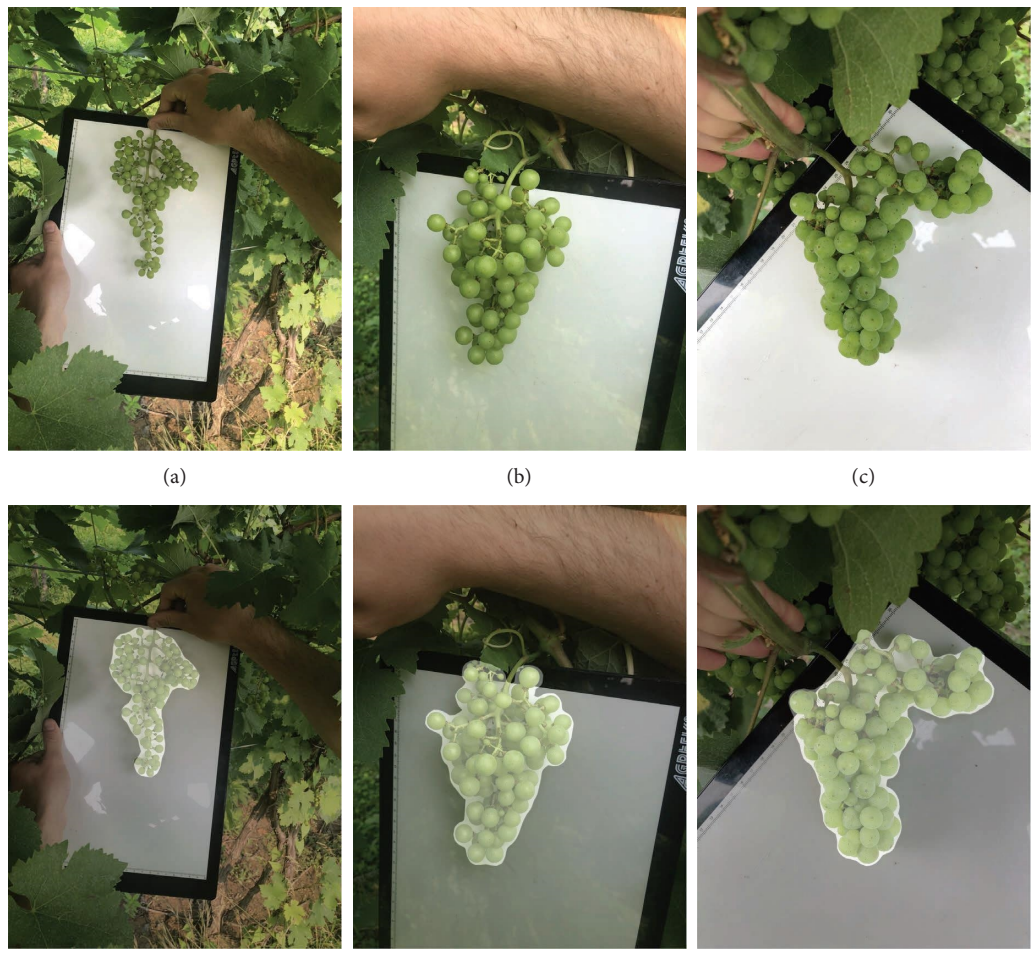

Figure 2: Examples of original images (a–c) in the dataset exhibit complexities such as varying zoom levels, the presence of unwanted objects (e.g., a hand), or similar objects in terms of shape and colour (e.g., canopy and clusters other than the intended one). These complexities have the potential to affect the segmentation process. Correspondingly, images (a1–c1) represent the segmented cluster boundaries generated using PSPNet, demonstrating its robustness in overcoming these challenges.

decreased the intensity variation within the berry pixels by other means. Thus, by lowering the intraclass variance of the berries class, the interclass variance between classes was maximized. The threshold value for left-shifted image distribution was optimal as it only captured the lower tail representing gap pixels (Figures 3(e) and 4). The contrast was increased only for compact cluster cultivars (Pinot gris and Riesling) for every timestep and not for looser clusters (Cabernet Franc).

After determining the automatic threshold value for each image, the images were converted into binary images with berry and gap pixels. The final percentage of CC was calculated using the equation as follows:

$$\%\ \text{cluster closure} = \left(\frac{\#\text{no of berry pixels}}{\#\text{no of gap pixels} + \#\text{no of berry pixels}}\right) \times 100. \tag{1}$$

It is important to note that using the abovementioned equation, the calculated % CC represents the expansion of the berry area over time rather than the shrinking gaps between berries, although these two aspects complement each other. The decision to focus on the degree of cluster closure in the context of berry expansion was solely the authors' choice to guide the discussion.

2.5. Statistical Analysis. Two main statistics were computed in this study using *R*. The first set of statistics comprised basic measures such as the mean and standard deviation of CC at each timestep. The second set involved fitting a curve between quantified CC and time. Based on the data pattern, an asymptotic regression approach was employed using the drc package in *R*, using the following curve equation:

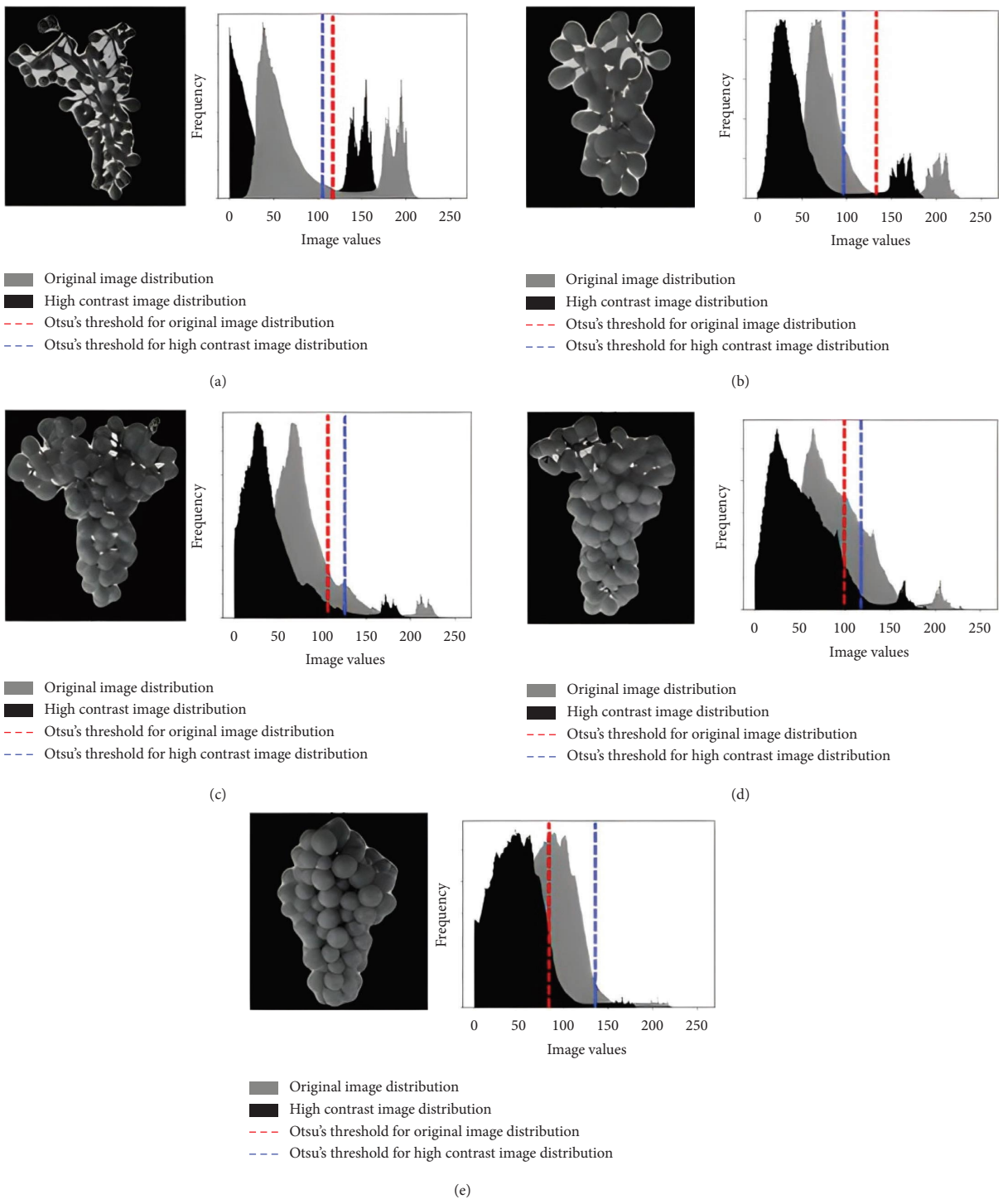

FIGURE 3: An example of Pinot gris clusters for histogram shifting and image thresholding representing the difference in Otsu's thresholding values between original and contrast images; (a–d) are images from June 29 to July 19 (E-L 27–32) where no difference was observed; (e) is an image of July 28 (E-L 33) where Otsu's threshold value for original image captures a larger portion of pixel values (>80), which can be the berry pixels, whereas for contrast images, the threshold value mainly captures the tail of pixel values (<120) representing gaps between the berries.

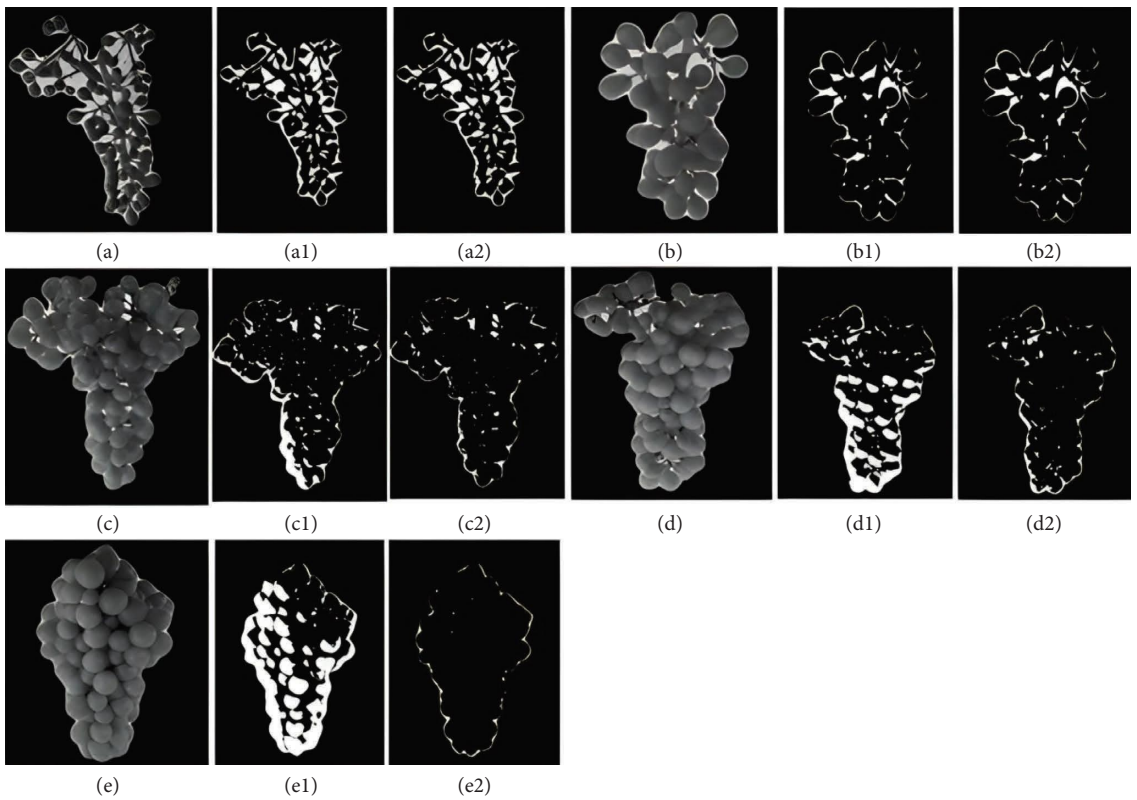

Figure 4: Comparison between final segmented images with and without enhancing contrast; (a–e) are grayscale images; (a1–e1) are final segmented images using original images (without enhancing contrasts); (a2–e2) are final segmented images using enhanced contrast images.

$$f(x) = a - (a\text{–}b).\quad \exp^{-CX}, \tag{2}$$

where a = asymptote, b = CC value when $x = 0$ (here x is number of weeks), and c represents the rate of progression in CC. These model parameters were quantified for each cultivar, and the corresponding x value was calculated for each cultivar, representing the time at which CC reached the asymptote.

3. Results

3.1. Delineating Cluster Boundaries. The PSPNet produced an overall mAcc of 0.98 and mIoU of 0.95. These results suggest that PSPNet provided a precise delineation of cluster boundaries regardless of other artifacts present in the images (Figure 2). Further analysis of individual class mIoU revealed that the mIoU was marginally higher for the noncluster class (0.98) than the cluster class (0.92). Both the precision and recall rate for the noncluster class was 0.99, and for the cluster class, it was 0.96.

3.2. Error in Quantification. Figure 5 illustrates an example of cluster progression as phenology advances, along with the quantified % CC for each image. Precise separation between berry and gap pixels was observed visually in almost every image for each cultivar, regardless of the phenological stage. However, a small percentage (<2%) of the whole image dataset resulted in inaccurate % CC. Specifically, 3% (7 out of 224) of Pinot gris images, 1% (3 out of 233) of Riesling images, and less than 1% (3 out of 325) of Cabernet Franc images falsely captured berries and gap pixels, leading to inaccuracies. Despite leading to a small number of images with inaccurately captured % CC, these images were incorporated into the modelling of % CC. This was done to assess the viability of the proposed method in tracking % CC throughout the growing season.

3.3. Temporal Variation in % CC. The mean % CC for Pinot gris was 80.3%, 90.3%, 94.2%, 93.5%, and 94.7% with standard deviations of 7.4%, 5.6%, 2.8%, 2.6%, and 2.1% across the phenological stages of June 29, July 6, July 12, July 19, and July 28, respectively (distribution of calculated % CC showed in Figure 6). For Riesling, the mean % CC for similar dates was 71.6%, 87.1%, 88.1%, 90.0%, and 93.6% with standard deviations of 9.2%, 7.2%, 5.2%, 5.9%, and 4.2%. The lower mean % CC by 1% for Pinot gris on July 19 compared to July 12 was due to a relatively higher number of falsely classified images (5 out of 7) that mistakenly identified brighter berry pixels as gap pixels, even after enhancing image contrast. Such effects were not observed for Riesling. For Cabernet Franc, the mean % CC ranged from 55.9% to 79.3% from July 2 to August 23. The standard deviation was 6-7% across all phenological stages. In general, compact cluster cultivars exhibited higher % CC values, ranging from 71% to 98%, compared to loose clusters with values ranging from 55% to 80%. Nonetheless, the range of mean % CC values for both types of clusters across the entire season was

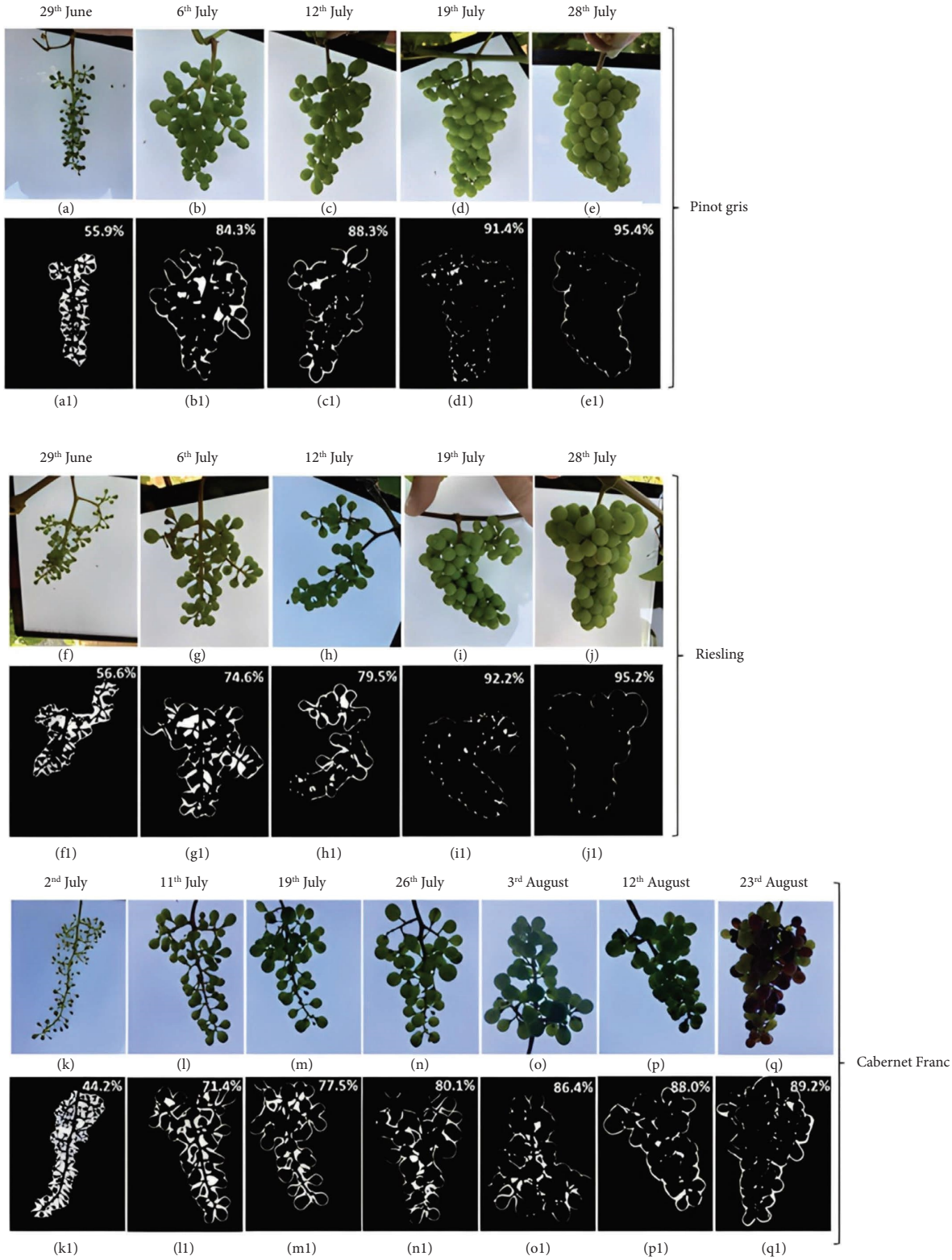

FIGURE 5: Examples of original images and final segmented images with % CC; (a–e) are the collected RGB images of Pinot gris, and (a1–e1) are final segmented images of these RGB images with % CC noted in the top right corner; similarly, (f–j) and (f1–j1) are Riesling, and (k–q) and (k1–q1) are Cabernet Franc.

similar, 27% for compact clusters and 25% for loose clusters. The differences in mean % CC at a particular phenological stage with respect to the next stage were 10.0%, 3.9%, 0.8%, and 1.2% for Pinot gris and 15.5%, 1.0%, 1.9%, and 3.6% for Riesling. Similarly, for Cabernet Franc, the progression was 7.1%, 12.9%, 3.2%, 0.6%, 1.0%, and 0.1% throughout the

season, indicating that clusters progress much faster towards closure early in the season, especially in the first two to three weeks, after which the % CC starts to reach an asymptote (Figure 6).

Table 1 presents the asymptote values for different cultivars, where Pinot gris had the highest value (94%) followed by Riesling (91%) and Cabernet Franc (81%). The time taken for Pinot gris to reach the asymptote was at 3.4 weeks, while Riesling took around 4 weeks. Cabernet Franc, however, did not reach the asymptote, although this could be due to the low-vigour vines in the block that were not necessarily representative of other blocks nearby. The progression rate (parameter c in equation (2)) was not significantly different between the compact cluster cultivars of Pinot gris (1.20%) and Riesling (1.19%), while it was almost half for the loose cluster of Cabernet Franc (0.58%). However, these model estimates are based on data comprising significant variation among clusters in % CC at any given time.

4. Discussion

The method outlined in the study has two notable advantages. First, unlike conventional cluster compactness methods that rely on the estimation of the number of berries per cm of rachis length [3], the developed approach is solely based on the gaps between berries. This independence from other viticulture parameters such as rachis length, number of berries, etc., makes the developed method less prone to errors caused by variations in cluster shape, size, or cluster morphology across cultivars. Second, the data collection method used in this study is nondestructive and requires minimal resources (i.e., a mobile phone and whiteboard). Given that the % CC metric employed in this study represents a percentage ratio between gap area and cluster area, there is no need for distance standardization in the image or the use of additional instruments for data collection. It allows for the tracking of cluster phenology under field conditions without the need for cluster removal from the vine or specific cluster selection.

In this study, the reduction in gaps serves as a proxy for the percentage of berry surface area that is in contact with other berries. It does not separate out the pedicel, peduncle, or flower pixels (seen in images in the first two weeks). This proxy measure or quantified % CC partially captures cluster compactness but only in later phenological stages (here after mid-July). However, such a proxy measure of CC for early phenological stages is limited by the overlay effect resulting from the 2D nature of the images. In 2D images, small berries may overlap each other, but due to the missing 3rd dimension (depth), it creates an illusion of berries touching each other causing a higher % CC. For instance, an image taken on July 2 of all cultivars in Figure 5 shows that the cluster is filled approximately 40–50%. However, the overlapping small berries and some flowers give the impression that the berries are touching each other, but in reality, there are few, if any, berries that are in contact with other berries. This could also be a possible cause of a large standard deviation of % CC for the early phenological stages compared to later stages for both Pinot gris and Riesling (as depicted in Figure 6). Specifically, for Pinot gris, the standard deviation in % CC on June 29 and July 6 was 7.4% and 5.6%, respectively, whereas it was less than 3% for later stages. Similarly, for Riesling, the deviations in % CC ranged from 7 to 10% for early phenological stages and 4-5% post-July 6. Note that we have captured only basal clusters, but a larger vineyard block, less uniform vines, and/or inclusion of distal clusters would potentially introduce more variability, but the method should reliably reflect that variability as long as the appropriate clusters are imaged. Going forward, it would be beneficial to address this limitation either by using depth cameras to capture cluster structures [29] or by first distinguishing the berry pixels from other pixels (such as pedicel, peduncle, and flowers) and subsequently identifying individual berries, as proposed by Aquino et al. [12]. Furthermore, Luo et al. [30] and Zabawa et al. [12] employed edge image processing to compute berry diameter and berry detection, respectively. This technique could potentially be refined and applied to determine the actual % CC by calculating the areas of berries touching each other and could be compared with the proposed method.

Despite this limitation, % CC can still be a useful tool for tracking the overall progression of CC because such overlay effects become marginal at the block level across the entire timeline. Our findings reveal that instead of viewing CC as a single phenological stage where the bunch is closed, it should be considered as a temporal progression of cluster phenology by means of the percentage of berry areas touching each other. CC progresses continuously throughout the season, leading up to veraison, and should be quantified as such. We used weeks as our X axis, but date/day of the year or thermal time could also be used.

The preliminary findings of this study suggest that a higher variation in quantified % CC during the first three weeks may indicate that clusters do not progress uniformly at the beginning of the season, but they eventually catch up later, reaching an asymptote. However, the time required to reach the asymptote is cultivar dependent. For instance, Pinot gris had a 3% higher asymptote than Riesling and reached the asymptote earlier (3.4 weeks) than Riesling (~4 weeks). This could be because the intercept parameter for Pinot gris was 42% at the beginning, which was almost twice that of Riesling (26%). However, loose clusters of low-vigour Cabernet Franc never reached an asymptote and progressed through veraison. Note that intercept should be used as a comparative mean across cultivars and not as an absolute value as it is a model estimate. Additional research is necessary to examine if the CC distribution varies within the cluster and whether that variation influences CC at the block level. It should be noted that this study aims to establish a user-friendly method for tracking cluster closure under field conditions. Therefore, the specific % CC trends for each cultivar should be considered as examples only; determining differences in % CC among cultivars would require additional investigation at multiple vineyard sites. Further investigations are needed to study this across more

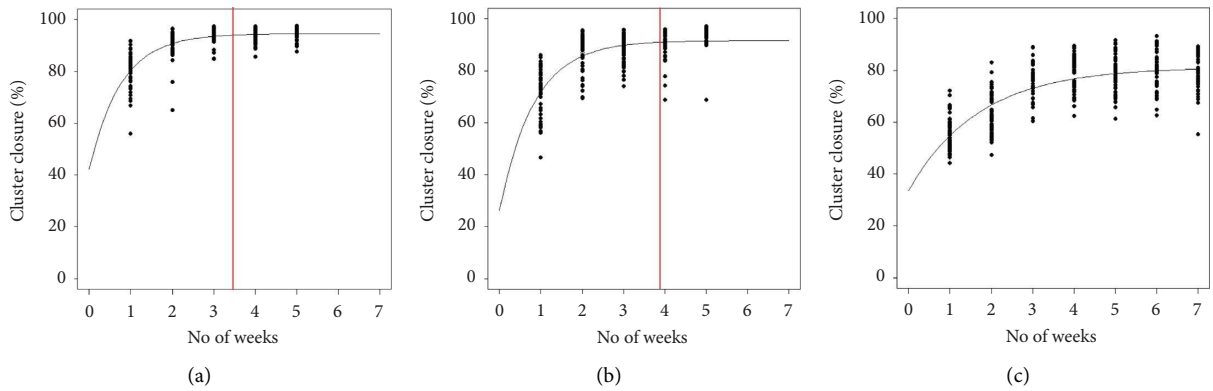

Figure 6: Temporal variation of quantified % CC; (a) Pinot gris; (b) Riesling; and (c) Cabernet Franc. The line represents the nonlinear regression model with an asymptote. The red line represents the time when it reaches the asymptote. Cabernet Franc (c) did not reach an asymptote. The *x*-axis represents the number of weeks after berry set (E-L stage 27).

Table 1: Asymptote regression model parameters for quantification of % CC in Pinot gris, Riesling, and Cabernet Franc.

Cultivars	Asymptote (parameter a in equation (2)	Intercept (parameter *b* in equation (2)	Rate of increase (parameter *c* in equation (2)	Time of cluster closure (weeks) as indicated by *X* value at asymptote
Pinot gris	94.58***	42.24***	1.29***	3.46
Riesling	91.61***	26.21	1.19***	3.90
Cabernet Franc	81.19***	33.68***	0.58***	—

The values with ***represent p value <0.001 using the t-test.

cultivars and also examine the effects of climate, crop load, weather, soil, and other environmental and biological factors that affect the progression of CC.

We propose using the method introduced in this paper as a research tool to address new and continuing discussions in viticulture. For instance, the infection of *Botrytis cinerea* in mature grapes is greatly influenced by wetness [31]. Young berries require an even shorter duration of wetness to cause infection [32], and vines at any stage of phenology starting as early as flowering are susceptible to such disease infection [33, 34]. In addition, disease severity is closely related to cluster compactness in mature grapes [2]; thus, this method can potentially be used as another variable in studies of interactions among the host, pathogen, and environmental conditions. Integrating this methodology with an automated system of cluster detection [35] could increase the spatial resolution and allow for finer temporal data, facilitating a more in-depth study of the variation in rapid cluster phenological progression.

Overall, this research provides an open-source tool to implement the methodology to quantify % CC directly, enabling the tracking of % CC progress in-field in a non-destructive manner (https://github.com/manushibt/Qunatifying-Grapevine-Cluster-Closure-QCC-.git).

5. Conclusion

This research presents a novel preliminary method for quantifying cluster closure (CC) and its timing and progression using image segmentation and image thresholding. The method, once validated at different sites and climates, will provide a tool for the progression of CC during the season with minimal field resources and open-source methodology, with less than 2% error in quantified % CC. Despite the limitation of inaccuracies in % CC during early phenological stages, the proposed method effectively captured the trend of % CC throughout the season for both cultivars with compact clusters and those with loose clusters. The % CC metric allows for further investigation of the relationship of CC to cluster compactness, disease susceptibility, and other parameters of interest in grape production. This research tool can be applied and validated for investigating CC progression in different cultivars and climates.

Data Availability

All images, data, and code have been posted to GitHub at (https://github.com/manushibt/Qunatifying-Grapevine-Cluster-Closure-QCC-.git).

Conflicts of Interest

The authors declare that they have no conflicts of interest.

Acknowledgments

We thank Yawen Lu for his early contributions to the image segmentation method. We heartily acknowledge the efforts of Jenn Russo, Justin Jackson, Anne Kearney, Michael Lovier, and Will Melancon for collecting the images of the clusters, Emily Grace Mcfadden and Mariam Patricia

Berdeja Aramayo for annotating the images, as well as 21 Brix Winery, Heart and Hands Wine Company, and Fulkerson Vineyards for their collaboration. We appreciate the helpful discussions offered by Dave Wiemann relating to this work. This work was supported by NSF grant #1837367 CPS: TTP Option: Medium: Touch Sensitive Technologies for Improved Vineyard Management and NIFA grant #1014705 Improving Vineyard Management Using Touch Sensitive Soft Robots.

References

[1] B. G. Coombe, "Growth stages of the grapevine: adoption of a system for identifying grapevine growth stages," *Australian Journal of Grape and Wine Research*, vol. 1, no. 1, 1995.

[2] F. M. Gabler, J. L. Smilanick, M. Mansour, D. W. Ramming, and B. E. Mackey, "Correlations of morphological, anatomical, and chemical features of grape berries with resistance to botrytis cinerea," *Phytopathology*, vol. 93, no. 10, pp. 1263–1273, 2003.

[3] B. Hed, H. K. Ngugi, and J. W. Travis, "Relationship between cluster compactness and bunch rot in vignoles grapes," *Plant Disease*, vol. 93, no. 11, pp. 1195–1201, 2009.

[4] A. Sepahi, "Estimating duster compactness in Yaghouti grapes," *VITIS J. Grapevine Res.*, vol. 19, pp. 81–90, 1980.

[5] T. Becker and M. Knoche, "Water induces microcracks in the grape berry cuticle," *Vitis J. Grapevine Res.*, vol. 51, pp. 141-142, 2012.

[6] M. E. Vail and J. J. Marois, "Grape Cluster Architecture and the Susceptibility of Berries to Botrytis Cinerea," *Phytopathology*, vol. 81, no. 2, 1991.

[7] International Organization of Vine and Wine (OIV), "OIV descriptor list for grape varieties and Vitis species," *Organ. Int. Vigne Vin Paris Fr. Section Buch Density*, International Organization of Vine and Wine, Dijon, France, 2007.

[8] A. Christodoulou, R. J. Weaver, and R. M. Pool, "Response of Thompson Seedless grapes to prebloom thinning," *VITIS J. Grapevine Res.*, vol. 6, p. 303, 1967.

[9] J. Tello and J. Ibáñez, "Evaluation of indexes for the quantitative and objective estimation of grapevine bunch compactness," *VITIS J. Grapevine Res.*, vol. 53, p. 9, 2014.

[10] A. Aquino, M. P. Diago, B. Millán, and J. Tardáguila, "A new methodology for estimating the grapevine-berry number per cluster using image analysis," *Biosystems Engineering*, vol. 156, pp. 80–95, 2017.

[11] L. M. Coviello, G. Cristoforetti, Jurman, and C. Furlanello, "GBCNet: In-field grape berries counting for yield estimation by dilated CNNs," *Applied Sciences*, vol. 10, no. 14, 2020.

[12] L. Zabawa, A. Kicherer, L. Klingbeil et al., "Detection of single grapevine berries in images using fully convolutional neural networks," 2019, https://arxiv.org/abs/1905.00458.

[13] B. Xin and M. Whitty, "A 3D grape bunch reconstruction pipeline based on constraint-based optimisation and restricted reconstruction grammar," *Computers and Electronics in Agriculture*, vol. 196, Article ID 106840, 2022.

[14] C.-Y. Huang, W.-T. Jheng, W.-K. Tai, C.-C. Chang, and D.-L. Way, "Procedural grape bunch modeling," *Computers and Graphics*, vol. 37, no. 4, pp. 225–237, 2013.

[15] F. Palacios, M. P. Diago, and J. Tardaguila, "A non-invasive method based on computer vision for grapevine cluster compactness assessment using a mobile sensing platform under field conditions," *Sensors*, vol. 19, no. 17, p. 3799, 2019.

[16] Q. Ye, H. Wang, and H. Li, "Lateral shoots removal has little effect on berry growth of grapevine (Vitis vinifera L.) 'Riesling' in cool climate," *Scientific Reports*, vol. 12, no. 1, Article ID 15980, 2022.

[17] S. Liu, X. Zeng, and M. Whitty, "3DBunch: a novel iOS-smartphone application to evaluate the number of grape berries per bunch using image analysis techniques," *IEEE Access*, vol. 8, pp. 114663–114674, 2020.

[18] E. Ivorra, A. J. Sánchez, J. G. Camarasa, M. P. Diago, and J. Tardaguila, "Assessment of grape cluster yield components based on 3D descriptors using stereo vision," *Food Control*, vol. 50, pp. 273–282, 2015.

[19] S. Cubero, M. P. Diago, J. Blasco et al., "A new method for assessment of bunch compactness using automated image analysis," *Australian Journal of Grape and Wine Research*, vol. 21, no. 1, pp. 101–109, 2015.

[20] J. Tello, S. Cubero, J. Blasco, J. Tardaguila, N. Aleixos, and J. Ibáñez, "Application of 2D and 3D image technologies to characterise morphological attributes of grapevine clusters," *Journal of the Science of Food and Agriculture*, vol. 96, no. 13, pp. 4575–4583, 2016.

[21] H. Zhao, J. Shi, X. Qi, X. Wang, and J. Jia, "Pyramid Scene parsing network," in *Proceedings of the IEEE Conference on Computer Vision and Pattern Recognition*, pp. 2881–2890, Honolulu, HI, USA, July 2017.

[22] N. Otsu, "A threshold selection method from gray-level histograms," *IEEE Transactions on Systems, Man, and Cybernetics*, vol. 9, no. 1, pp. 62–66, 1979.

[23] L.-C. Chen, G. Papandreou, F. Schroff, and H. Adam, "Rethinking atrous convolution for semantic image segmentation," 2017, https://arxiv.org/abs/1706.05587.

[24] Y. Liu, L. Chu, G. Chen et al., "PaddleSeg: a high-efficient development toolkit for image segmentation," 2021, https://arxiv.org/abs/2101.06175.

[25] P. Jaccard, "Etude de la distribution florale dans une portion des Alpes et du Jura," *Bulletin de la Societe Vaudoise des Sciences Naturelles*, vol. 37, pp. 547–579, 1901.

[26] C. R. Harris, K. J. Millman, S. J. van der Walt et al., "Array programming with NumPy," *Nature*, vol. 585, no. 7825, pp. 357–362, 2020.

[27] G. Bradski, "The OpenCV library," 2000, https://opencv.org/.

[28] J. Kittler and J. Illingworth, "On threshold selection using clustering criteria," *IEEE Transactions on Systems, Man, and Cybernetics*, vol. 15, no. 5, pp. 652–655, 1985.

[29] B. Parr, M. Legg, and F. Alam, "Analysis of depth cameras for proximal sensing of grapes," *Sensors*, vol. 22, no. 11, p. 4179, 2022.

[30] L. Luo, W. Liu, Q. Lu et al., "Grape berry detection and size measurement based on edge image processing and geometric morphology," *Machines*, vol. 9, no. 10, p. 233, 2021.

[31] J. Broome, "Development of an infection model for botrytis bunch rot of grapes based on wetness duration and temperature," *Phytopathology*, vol. 85, no. 1, p. 97, 1995.

[32] N. G. Nair and R. N. Allen, "Infection of grape flowers and berries by Botrytis cinerea as a function of time and

temperature," *Mycological Research*, vol. 97, no. 8, pp. 1012–1014, 1993.

[33] N. Ciliberti, M. Fermaud, L. Languasco, and V. Rossi, "Influence of fungal strain, temperature, and wetness duration on infection of grapevine inflorescences and young berry clusters by botrytis cinerea," *Phytopathology*, vol. 105, no. 3, pp. 325–333, 2015.

[34] G. N. Hill, K. J. Evans, and R. M. Beresford, "Use of nitrate non-utilizing (nit) mutants to determine phenological stages at which Botrytis cinerea infects wine grapes causing botrytis bunch rot," *Plant Pathology*, vol. 63, no. 6, pp. 1316–1325, 2014.

[35] L. Ghiani, A. Sassu, F. Palumbo, L. Mercenaro, and F. Gambella, "In-field automatic detection of grape bunches under a totally uncontrolled environment," *Sensors*, vol. 21, no. 11, p. 3908, 2021.